https://doi.org/10.5194/egusphere-2025-5536
Preprint. Discussion started: 3 December 2025

High temporal resolution photos of SAR arc rays lead to a new interpretation of the physical causes: Wave-particle interactions and energetic electron precipitation

Bruce T. Tsurutani[1,*], Gurbax S. Lakhina[2,**], Rajkumar Hajra[3], Richard B. Horne[4], Masatomi Iizawa[5], Yasuhito Narita[5], Ingo von Borstel[6], Karl-Heinz Glassmeier[6], Volker Bothmer[7], Klaus Reinsch[7], Philipp Schulz[8], and Sami Solanki[9]

[1]Jet Propulsion Laboratory, California Institute of Technology, Pasadena, California, USA
[2]Indian Institute of Geomagnetism, Navi Mumbai, India
[3]CAS Key Laboratory of Geospace Environment, School of Earth and Space Sciences, University of Science and Technology of China, Hefei, People's Republic of China
[4]British Antarctic Survey, Cambridge, England
[5]Institut für Theoretische Physik, Technische Universität Braunschweig, Braunschweig, Germany
[6]Institut für Geophysik und Extraterrestrische Physik, Technische Universität Braunschweig, Braunschweig, Germany
[7]Institut für Astrophysik und Geophysik, Georg-August-Universität Göttingen, Germany
[8]Fraunhofer-Institut für Schicht-und Oberflächentechnik IST, Braunschweig, Germany
[9]Max-Planck-Institut für Sonnensystemforschung, Göttingen, Germany
[*]Retired, Pasadena, California, USA
[**]Retired, Navi Mumbai, India

Correspondence: Y. Narita (y.narita@tu-braunschweig.de)

Abstract. High spatial and temporal resolution images of red auroras over Germany during the 10–11 May 2024 magnetic storm have added new information concerning stable auroral red (SAR) arc formation. The high-altitude red aurora displayed brightness streaks/rays, which continued to lower altitude green auroral brightness rays, indicating that energetic electron precipitation along the Earth's magnetic field lines are causing both auroras. Both the red and green auroras are diffuse in nature, indicating that instability of high-energy ring current particles inside the plasmasphere followed by wave-particle interactions is the most likely cause of the precipitating electrons. The 5577Å diffuse green aurora below the SAR arcs is a new scientific finding. This is named Stable Auroral Green (SAG) arcs. The SAR and SAG arc images were taken during the first and second steps of the 2024 superstorm. They occurred during intense substorms.

1 Introduction

Stable Auroral Red (SAR) arcs have presumably been seen since the beginning of mankind. They were noted just prior to the French revolution and the blood red color of the metastable oxygen 6300 Å line of a SAR arc was taken as an omen for future bloodshed. During 1957–1958, a particularly strong geomagnetically active interval, SAR arcs were seen ∼20% of the time (Roach and Roach, 1963). Scientific studies have found that the red aurora occurs during intense magnetic storms at altitudes spanning from ∼200 km to ∼800 km with a maximum intensity at ∼370–400 km (Barbier, 1958; Roach and Marovich, 1959).

https://doi.org/10.5194/egusphere-2025-5536
Preprint. Discussion started: 3 December 2025

SAR arcs are observed at mid- and low-latitudes, are long-lasting (∼10 hrs), and are believed to form rings around the Earth in both the north and south hemispheres at roughly constant magnetic latitudes (see review in Roach and Roach, 1963). SAR arcs are described as "stable" because their displays are essentially constant, while auroras in the near-polar auroral zones during magnetic storms are highly variable in both location and time.

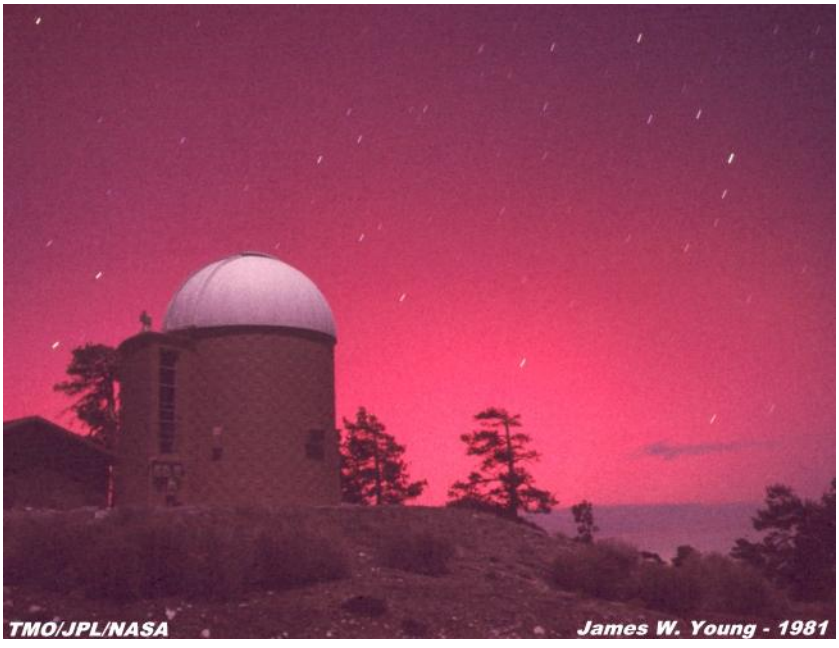

Figure 1. A red aurora that occurred during 12 April 1981 slightly north of Los Angeles, California. In the foreground is the Jet Propulsion Laboratory, California Institute of Technology (also NASA) observatory at Table Mountain in the mountains north of Los Angeles. This is a typical older red aurora image. The picture was taken by James Young a scientist who was studying the moon Io (of Jupiter) at the time.

An example of a low-latitude red aurora observed near Los Angeles, California in 1981 is shown in Figure 1. During the 11:00 pm local television newscast, the announcer told viewers to go outside and experience the unusual red aurora. It must have been quite bright to have been seen by the naked eye (∼100 R is the threshold for natural visibility). This is a typical sighting of a red aurora. Notice that no red auroral rays nor green auroras (discussed later in the paper) are apparent from this image. The exposure time of this image was not recorded, but because the stars appear as "streaks", the exposure was reasonably long. The image was taken with the use of a tripod.

Los Angeles is at a magnetic latitude of 41.0°. 11:00–11:30 pm on 12 April Los Angeles local time (LT) was 06:00–06:30 UT on 13 April. Figure 2 shows the interplanetary/solar wind and geomagnetic conditions during the red aurora observation. The near-Earth (shifted to the Earth's bow shock nose) solar wind plasma and interplanetary magnetic field (IMF) data (temporal resolution of 1 hr) measured by upstream spacecraft are obtained from NASA's OMNIweb (King and Papitashvili, 2020). The symmetric ring current index (Dessler and Parker, 1959; Sckopke, 1966; Iyemori, 1990) SYM-H (1 min resolution) is obtained from t he World Data Center for Geomagnetism, Kyoto, Japan, and the auroral electrojet indices SME and SML (1 min) are

https://doi.org/10.5194/egusphere-2025-5536
Preprint. Discussion started: 3 December 2025

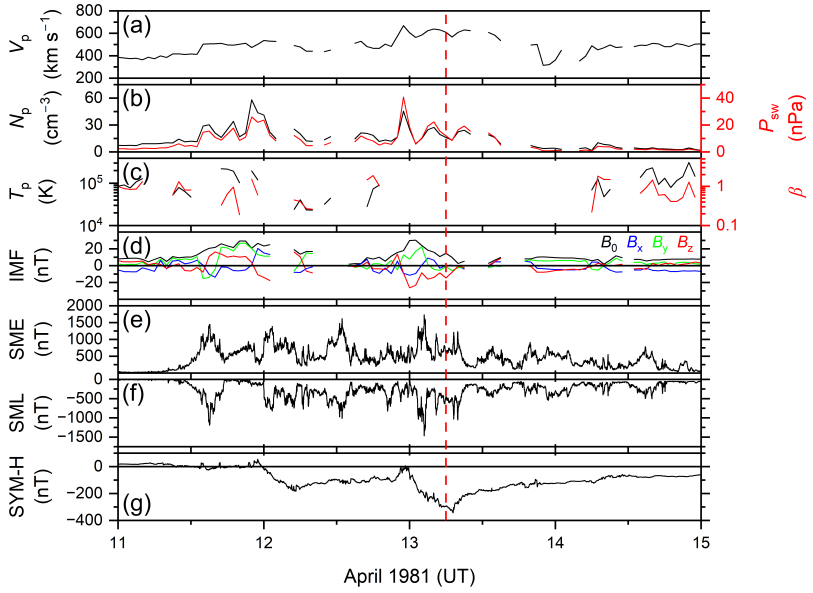

Figure 2. The solar wind data and geomagnetic activity indices for the magnetic storm during 11–14 April 1981. From top to bottom, the panels are: (a) solar wind proton speed Vp, (b) proton density Np (black, legend on the left) and ram pressure Psw (red, legend on the right), (c) proton temperature Tp (black, legend on the left) and plasma-β (red, legend on the right), (d) interplanetary magnetic field (IMF) magnitude B_0, and B_x, B_y, and B_z components, (e) auroral electrojet index SME, (f) auroral electrojet index westward component SML, and (g) symmetric ring current index SYM-H. The solar/interplanetary parameters (a–d) have time resolution of 1 hr, and the geomagnetic indices (e–g) have time resolution of 1 min. The red aurora viewing time near Los Angeles, California is marked by a vertical gray shading (11:00–11:30 pm local time).

taken from SuperMAG (Gjerloev, 2009, 2012; Newell and Gjerloev, 2011). The vertical gray shading in Figure 2 indicates the approximate time of the red aurora television announcement (11:00–11:30 LT or 06:00–06:30 UT). The geomagnetic storm was a two main phase (or two SYM-H peak) magnetic storm. The first peak occurred at ∼05:17 UT on 12 April with a SYM-H intensity of -184 nT. The second storm peak was at ∼07:09 UT on 13 April with a SYM-H = -343 nT value. Although the solar wind data had many gaps and was low time resolution, it appears that both storms were caused by southward IMF B_z values. Magnetic reconnection between the solar wind B_z fields and the Earth's magnetopause fields is the cause of energy transfer from the solar wind to the magnetosphere (Dungey, 1961; Tsurutani et al., 1988; Echer et al., 2008).

At the beginning time of the Los Angeles newscast, the storm time ring current index SYM-H was -294 nT (Figure 2g). The red aurora occurred during the storm second main phase, slightly (∼1 hr 11 min) before the storm peak intensity. The SME (Figure 2e) and SML (Figure 2f) indices indicate strong substorm activity. The physical mechanism for the excitation of high-altitude oxygen atoms for the creation of red auroras has been debated in literature. Cole (1965) suggested that the storm-time ring current electrons and ions transfer energy to neutral particles via Coulomb collisions to heat the thermal plasma to

https://doi.org/10.5194/egusphere-2025-5536
Preprint. Discussion started: 3 December 2025

temperatures of ∼104 K. Heat conduction down the magnetic field lines of force create the red aurora. Rees et al. (1967) and Rees (1989) suggested precipitation of ∼1 to 4 keV electrons along geomagnetic field lines produce secondary non-ionizing electrons which excite oxygen atoms to a metastable state. Cornwall et al. (1970, 1971) suggested that during the magnetic storm recovery phases, the plasmasphere begins to physically enlarge itself from its shrunken storm-time state, bringing the high density $\sim 10^3\,\mathrm{cm}^{-3}$ thermal plasmaspheric plasma over the ring current energetic particles. This leads to an instability of the ring current ions and the growth of ion cyclotron waves. The ion cyclotron waves, then by Landau damping of the waves, accelerate thermal electrons to suprathermal energies. The suprathermal electrons excite the oxygen atoms to their metastable states. More recently, Kozyra et al. (1993) have proposed that it is energetic ring current oxygen ions which are the ultimate source for SAR arcs. Collisions between these energetic ions and thermal plasmaspheric electrons energize the electrons. The energized electrons in turn stimulate the oxygen atoms to their excited metastable states.

Very recently, a rare magnetic storm occurred during 10–12 May 2024. The magnetic storm had three sub-main phases with peak SYM-H intensities of: -183, -354, and -518 nT (Hajra et al., 2024). This was the second highest peak intensity magnetic storm that has occurred during the space age (since 1957). It is well known that the storm-time convection electric fields will transport energetic electrons and ions to very low L shells ($L < 3.0$) and auroras can be noted at these distances (Tsurutani et al., 2003; Tsurutani and Lakhina, 2014). L is defined as the distance in Earth radius (RE) for a dipole magnetic field line to cross the magnetic equatorial plane (McIlwain, 1961). It is the purpose of this paper to show high time resolution auroral observations taken from the ground at Braunschweig and Göttingen, Germany, identifying several new features of SAR arcs. We will also discuss, for the first time, related Stable Auroral Green (SAG) arcs.

2 Results

Auroras were seen over Germany between ∼19:00 and 24:00 UT (and perhaps longer) on 10 May 2024. The image in Figure 3 was taken at ∼22:16 UT. Braunschweig is at a magnetic latitude (MLAT) of 52.2°. The photo was taken by a Google Pixel 7 (6.81 mm), Ultra HDR, standard zoom, f-stop 1.85 and ISO 9338. The exposure time was 6 s. Notice the stars appear as points compared to the streaks in Figure 1.

Several interesting features are noted in this closeup of the aurora shown in Figure 3. The red portion of the aurora is not a featureless reddish display similar to the aurora shown in Figure 1, but there are rays in the red auroras from the upper right downward slightly to the left. This has never been reported before in scientific articles, to our knowledge. Another new feature is the green oxygen 5577 Å display below and to the left of the red aurora. The rays in the red aurora are continued into the green aurora. The rays are enhancements in brightness. In general, the green aurora is featureless other than the rays. This also has never been reported before. We call these Stable Auroral Green or SAG auroras. This latter feature is interpreted as energetic electrons streaming down the Earth's magnetic field lines (the straight lines) causing both the red and the green auroras.

The SAG auroras are "featureless" in that they do not have ∼1 km width arcs or ribbons like those that occur in auroral zone (65° to 70°) green auroras.

https://doi.org/10.5194/egusphere-2025-5536
Preprint. Discussion started: 3 December 2025

Figure 3. An SAR arc aurora detected over Braunschweig, Germany on 10 May 2024. Notice the parallel rays in both the red and green auroras. The photo was taken by Philipp Schulz. The center of the photo is pointed in the east-northeast direction. Cygnus and Lyra constellations are visible.

Why is this image so different from the Los Angeles red auroral image shown in Figure 1? If one realizes the extreme potential height (∼800 km) of the red aurora, the aurora can be occurring some distance poleward of the viewing location. An ∼800 km red aurora viewed at the horizon will translate into the aurora occurring ∼13° in magnetic latitude away (Los Angeles at 41° MLAT is ∼11° lower in MLAT than Braunschweig at ∼52° MLAT). Due to the curvature of the Earth (and the local mountains), any potential green aurora would not be seen by the Los Angeles viewers. Only in an extreme magnetic storm like the 10–11 May 2024 event, where the auroras occurred over Germany, can the green auroral portions be observed. We also note that the SAR arc in Figure 1 was taken with a long-time exposure so that the rays were probably time-averaged out. The large distance between Los Angeles and the red aurora is another factor in not being able to distinguish rays.

Figure 4 shows another interesting feature of the red and green aurora taken at 22:49 UT. The view is to the north-east direction. The picture was taken by a Canon R6 Mark II with a Canon L Zoom 14–35 mm lens. A tripod was used with the lens at 16 mm, an f-stop of 4 and a 6 sec exposure. The ISO setting was 2500. Göttingen is at 51.6° MLAT.

Figure 4 shows that both the red and green rays were again enhanced brightness regions. The red rays continue down to lower altitude green rays. There is an apparent gap between the red and green aurora. The rays from the red to green auroras are present, but there is a dimming in between.

The image in Figure 5 was taken at 19:43 UT at Göttingen, Germany, some ∼2.5 to 3 hrs prior to the images of Figures 3 and 4. At the time of Figure 5, the magnetic storm main phase was less intense than during the prior figures. Figure 5

https://doi.org/10.5194/egusphere-2025-5536
Preprint. Discussion started: 3 December 2025

Figure 4. A red and green aurora taken over Göttingen, Germany. The photo was taken by Sami Solanki.

shows a different relationship between the SAR and SAG auroras. The two types of auroras are separate. There is no SAG arc visible beneath the SAR arc and there is no SAR arc above the SAG arc. Rays are not visible in either SAG or SAR arcs. One possible interpretation is that both the SAG and SAR arcs are distant features making the viewing of rays difficult. A possible explanation of the separation of the SAG and SAR arcs is that the SAR arc is on magnetic field lines within the plasmasphere and the SAG aurora is on magnetic field lines just outside of the plasmasphere.

Figure 6 shows the complex interplanetary causes of the 10–11 May 2024 magnetic storm. The fast forward shock at 17:05 UT and magnetosonic wave at 22:09 UT on 10 May were identified using the Abraham-Shrauner (1972) shock normal criteria and the Rankine-Hugoniot conservation equations (Rankine, 1870; Hugoniot, 1887, 1889). The shock magnetosonic Mach number was determined to be 7.15 and the magnetosonic wave had a Mach number of 0.55. Four magnetic cloud (MC) intervals were identified examining the plasma-β and IMF variations together. The times of the four MCs are: ∼20:50 UT on 10 May to ∼00:23 UT on 11 May (MC1) ∼03:05 to ∼07:55 UT on 11 May (MC2); ∼08:15 to ∼10:07 UT on 11 May (MC3);

https://doi.org/10.5194/egusphere-2025-5536
Preprint. Discussion started: 3 December 2025

Figure 5. An SAR and SAG aurora taken in Göttingen, Germany. The SAR arc is in the center of the image and the SAG arc is on the right. The direction of the image is 288° in azimuth or the west-north-west direction. The picture was taken with a Canon EOS M, an 8 mm Fish-Eye lens, and a f-stop of 2.8. The exposure time was 8 sec. The ISO was 800. The picture was taken by Klaus Reinsch at 19:43 UT.

and ∼11:53 to ∼17:26 UT on 11 May (MC4). The times of the three SAR arc sightings are indicated in Figure 6g by black triangles.

The storm main phase occurred in three primary steps with peak intensities of SYM-H = -183 nT, -354 nT and -518 nT, as previously mentioned. They were caused by southward IMF B_z with intensities -40 nT, -43 nT and -71 nT (see detailed discussion in Hajra et al., 2024). The first storm main phase step was caused by sheath interplanetary southward B_z fields. The second storm main phase step was caused by MC IMF B_z southward fields. The third step was presumably due to southward B_z fields in sheath plasma. The auroral observations in Figures 5, 3, and 4 occurred between ∼19:00 and 23:00 UT on 10 May. The SAR arc observation time in Figure 5 is indicated by the far-left triangle. This corresponds to the first step of the main phase storm extending into the beginning of the second step of the main phase storm. The time of the SAR arc observation occurs during a supersubstorm (SSS; Tsurutani et al., 2015) of intensity SML = -4456 nT (Figure 6f) triggered by an abrupt IMF B_z southward excursion of -18 nT (Figure 6d) (see Hajra et al., 2025, for a detail discussion of all SSSs occurring during the May 2024 superstorm). The Figure 5 SAR arc was observed during a small positive increase in the SYM-H index. The SAR arcs in Figures 3 and 4 (the second and third triangles from the left) occurred in the second step of the magnetic storm main phase when the SYM-H value was relatively constant. The Figure 3 SAR arc image was taken at the time of the interplanetary magnetosonic wave impact and the start of a substorm. The Figure 4 SAR arc image was taken during the substorm with a peak intensity of SML = -2450 nT at 22:40 UT. There were videos taken from the Deutsches Museum in Munich, Germany. The magnetic latitude is 48.0°. The website to access the videos is https://www.youtube.com/watch?v=JDBEyiOdo8U. What is interesting is that the videos state that the green aurora was “diffuse”.

https://doi.org/10.5194/egusphere-2025-5536
Preprint. Discussion started: 3 December 2025

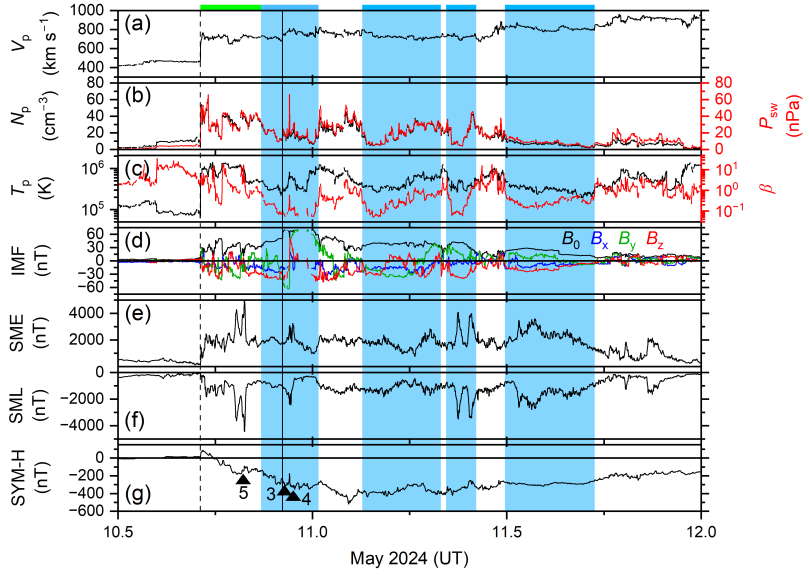

Figure 6. Solar wind/interplanetary and geomagnetic conditions during the 10–11 May 2024 storm. The panels are in the same format as in Figure 2. Vertical lines indicate an interplanetary fast forward shock (dashed line) and a magnetosonic wave (not a shock; solid line) impingement times. An interplanetary sheath is marked by a green bar at the top. Four magnetic clouds (MCs) are marked by vertical light-blue shadings and horizontal bars at the top. Black triangles in the SYM-H panel indicate auroral image times. From left to right the triangles indicate SAR arc images shown in Figures 5, 3, and 4, respectively (the triangles are numbered accordingly).

3 Some Background Information on Red (SAR) and Green (SAG) Auroras

Red auroral lines are caused by the decay of an oxygen atom meta-stable state (^{1}D) to the ^{3}P state. This meta-stable state is long lived with a lifetime of ∼110 sec. The emissions occur at 6300 Å and lesser at 6364 Å (630.0 and 636.4 nm). The green aurora is also associated with the decay of a metastable state of oxygen atoms, from the ^{1}S state into the ^{1}D state. The mean lifetime of the ^{1}S state is ∼0.74 sec. The decay is the well-known green 5577 Å (557.7 nm) line. The auroral green line is typically the brightest line seen in auroras in the high latitude auroral zone (65° to 70° magnetic latitudes). The activation of these meta-stable states of oxygen is due to electron collisions. The probability for the excitation into one of these states depends on the collision cross section σ. Above a few 100 eV is the so-called Bethe-regime with $\sigma \propto 1/E$, where E is the electron energy. Typical values of σ are:

Electron energy	σ[O(^{1}D)]	σ[O(^{1}S)]
20 eV (measured)	1.5×10^{-17}cm^2	$\sim 2 \times 10^{-18}$cm^2
1 keV (extrapolated)	$\sim 1 \times 10^{-18}$cm^2	$\sim 2 \times 10^{-19}$cm^2
10 keV (extrapolated)	$\sim 2 \times 10^{-19}$cm^2	$\sim 2 \times 10^{-20}$cm^2

https://doi.org/10.5194/egusphere-2025-5536
Preprint. Discussion started: 3 December 2025

With these cross-section values we can determine the probability of an excitation per path length: $n\dot{\sigma}$ where n is the density of atoms. For example, an electron with 20 eV kinetic energy has a $\sigma \approx 10^{-17}\mathrm{cm}^2$. The oxygen atomic density at a height of 200 km is 10^{11} atom cm^{-3}. Thus, a path length at this height would be 1 cm. These results (after some further considerations) are a probability of 10^{-6} for an excitation. Thus, we need many electrons to get a suitable number of excited atoms to cause bright auroral activity. The low probability furthermore implies that a single keV electron can cause many excitations. However, it is noted from the above σ values that the values decrease with increasing electron energy.

An important process we need to consider is quenching or collisional deexcitation, the deactivation of the oxygen metastable state by collisions with other atoms and molecules, for example, nitrogen. Quenching implies that the oxygen atom returns to its ground state without emitting a photon. A typical quenching reaction is: $\mathrm{O}(^1\mathrm{D}) + N_2 \rightarrow \mathrm{O} + \mathrm{N}_2$. Thus, quenching strongly depends on the nitrogen molecular density. At heights above 200 km this density is low and quenching does not occur. This implies that the long-living $\mathrm{O}(^1\mathrm{D})$ oxygen atoms have a high probability of emitting red photons. Below about 180 km the nitrogen density increases. Emission is no longer possible because of significant quenching of the $\mathrm{O}(^1\mathrm{D})$ atom. This is the reason why red auroras are typically occurring at heights above 200 km. Oxygen atoms decaying from the ^{1}S state have a much shorter lifetime. Thus, they are not as vulnerable to quenching as from $\mathrm{O}(^1\mathrm{D})$. Within a lifetime of $\sim$0.74 sec the chances of a stimulated oxygen atom to collide with a nitrogen molecule is low. Thus, metastable oxygen ^1S states can survive in even denser atmospheric environments. This is the reason why green auroral emissions occur much lower in the atmosphere than the red emissions. Only below a height of $\sim$90 km are atmospheric densities high enough to cause quenching.

4 Summary of observations

1. Modern high-speed camera images of SAR arcs over Germany during an intense magnetic storm showed parallel linear red auroral brightness rays, indicating that they were created by precipitating energetic electrons traveling along magnetic field lines.

2. The red auroral rays continued to lower altitude green auroral rays indicating that both the red and green auroras were caused by the same magnetospheric/ionospheric phenomenon.

3. The green auroras were diffuse and have been named SAG arcs. Diffuse auroras (Thorne, 2010) are caused by magnetospheric equatorial pitch angle scattering of energetic electrons into the loss cone, propagating down the magnetic fields and loss to the atmosphere.

4. The SAR and SAG arcs over Germany were detected in the first and second steps of the three-step main phase of a very intense magnetic storm.

5. The SAR arc in Figure 5 occurred during a supersubstorm of peak intensity SML = -4456 nT and in a slight recovery of the SYM-H indices. The SYM-H index was ~ -180 nT at the time of the image.

https://doi.org/10.5194/egusphere-2025-5536
Preprint. Discussion started: 3 December 2025

6. The SAR arcs in Figures 3 and 4 occurred during a relative flat portion of the second step of the storm main phase and at the beginning and in the intense portion of a substorm of peak intensity SML = -2450 nT.

7. Previous observations of SAR arcs such as in Figure 1 were often distant observations with long time exposures. The observation of the SAR and SAG arcs of Figure 3 also did not show rays even though the picture exposure time was only 8 sec. Thus, it is speculated that it is the long distance from the auroras and the low spatial resolution incurred that cause the loss of being able to distinguish SAR arc rays.

5 Discussion

The observation of continuous rays in the SAR and SAG arcs observed over Germany during the 10–11 May 2024 superstorm can discount previously proposed mechanisms and offer a new one. The bright ray enhancements show that energy is directly deposited at altitudes between ∼800 km and ∼100 km (and below) by energetic electron precipitation. This rules out the mechanism of Coulomb collision of ring current protons with plasmaspheric ions and heat conduction flowing down the magnetic field lines as proposed by Cole (1965). The presence of the rays in the SAR arcs is contrary to the idea of Landau damping of electromagnetic ion cyclotron waves produced by anisotropic ring current protons (Cornwall et al., 1970, 1971). The rays spatially continuing from the SAR arcs into the SAG arcs are contrary to the proposed idea that the SAR arcs are caused by energetic ring current oxygen ions (Kozyra et al., 1993). It is well known that green aurora rays are produced by energetic precipitating electrons (Lummerzheim, 2007). Finally, there is the Rees et al. (1967) proposal that ∼1 to 4 keV precipitating electrons are creating secondary electrons which then stimulate oxygen atoms into their elevated metastable states. Such low energy electrons are “monoenergetic” (Evans, 1974) and are now known to be accelerated in double layers a few RE above the surface of the Earth (Block, 1978; Lemaire and Scherer, 1974; Carlson and Kelley, 1977). Hasegawa (1976) suggests that a parallel electric field component of the kinetic Alfvén wave is causing the electron acceleration. Schriver et al. (2003) have suggested other auroral acceleration processes. The precipitation from acceleration in double layers forms discrete auroras of ∼km width arcs, not diffuse auroras. Thus, the Rees et al. (1967) mechanism can be discounted.

The three images of SAR arcs (Figures 5, 3 and 4) occurred when SYM-H was increasing slightly (Figure 5) or when SYM-H was relatively flat (Figures 3 and 4). All occurred during intense substorm intervals. We speculate that substorm convection electric fields are separate and distinct from magnetic storm convection electric fields (Tsurutani and Gonzalez, 2007). If this is correct, the substorm electric fields have injected plasmasheet particles into the high plasma density plasmasphere, leading to the SAR arcs. Although there are only a few observations of this provided here, further SAR arc studies can either confirm or deny this possibility.

6 Final comments

What are the waves that scatter the ring current electrons into the loss cone and the instability that creates the plasma waves? Smith et al. (1974) showed that electromagnetic plasmaspheric hiss was not present during a magnetic storm main phase at

https://doi.org/10.5194/egusphere-2025-5536
Preprint. Discussion started: 3 December 2025

local noon, ruling out an energetic electron loss cone/temperature anisotropy instability at that local time. What is detected at and near the plasmapause during strong geomagnetic activity are magnetosonic waves generated by an ion ring distribution instability (Gurnett, 1976; Perraut et al., 1982; Boardsen et al., 1992; Horne et al., 2000; Santolík et al., 2002; Meredith et al., 2008; Pokhotelov et al., 2008; Němec et al., 2013). Tsurutani et al. (2014) showed details of magnetosonic waves during a substorm at local midnight. The waves were linear polarization with exceptionally large Ew = ±25 mV/m electric oscillations perpendicular to B0 and large Bw = ±1 nT magnetic components parallel to B_0. Plasmaspheric hiss was detected away from the magnetic equator. It is possible that both the magnetosonic wave electric field oscillations and the plasmaspheric hiss are leading to energetic electron pitch angle diffusion into the loss cone. If the precipitating electrons are indeed hundreds of keV ring current particles, bremsstrahlung X-rays should be produced which in turn may cause interesting ionospheric and atmospheric effects below.

Data availability. The near-Earth solar wind plasma and IMF data are obtained from NASA's OMNIWeb Plus database https://omniweb.gsfc.nasa.gov/. The 1-hr and 1-min data can be directly downloaded from the pages: https://omniweb.gsfc.nasa.gov/form/dx1.html and https://omniweb.gsfc.nasa.gov/form/omni_min.html, respectively, by specifying start and stop times, and required plasma and IMF parameters.

Code and data availability. No codes or data are used in this work.

Author contributions. Conceptualization: Bruce T. Tsurutani
Data curation: Philipp Schulz, Sami Solanki, Klaus Reinsch, Rajkumar Hajra, Bruce T. Tsurutani
Formal analysis: Bruce T. Tsurutani, Rajkumar Hajra, Gurbax S. Lakhina, Karl-Heinz Glassmeier, Masatomi Iizawa, Richard B. Horne, Yasuhito Narita, Ingo von Borstel, Volker Bothmer
Funding acquisition: Rajkumar Hajra
Investigation: Bruce T. Tsurutani, Gurbax S. Lakhina, Rajkumar Hajra, Yasuhito Narita, Richard B. Horne, Masatomi Iizawa, Ingo von Borstel, Volker Bothmer, Karl-Heinz Glassmeier, Klaus Reinsch, Philipp Schulz, Sami Solanki
Methodology: Bruce T. Tsurutani, Rajkumar Hajra, Gurbax S. Lakhina, Karl-Heinz Glassmeier, Richard B. Horne, Masatomi Iizawa
Resources: Philipp Schulz, Sami Solanki, Klaus Reinsch, Rajkumar Hajra, Bruce T. Tsurutani, Volker Bothmer, Ingo von Borstel
Supervision: Bruce T. Tsurutani, Rajkumar Hajra, Yasuhito Narita Validation: Bruce T. Tsurutani, Gurbax S. Lakhina, Rajkumar Hajra, Yasuhito Narita, Richard B. Horne, Masatomi Iizawa, Ingo von Borstel, Volker Bothmer, Karl-Heinz Glassmeier, Klaus Reinsch, Philipp Schulz, Sami Solanki
Visualization: Philipp Schulz, Sami Solanki, Klaus Reinsch, Volker Bothmer, Ingo von Borstel
Writing – original draft: Bruce T. Tsurutani
Writing – review & editing: Bruce T. Tsurutani, Gurbax S. Lakhina, Rajkumar Hajra, Yasuhito Narita, Richard B. Horne, Masatomi Iizawa, Ingo von Borstel, Volker Bothmer, Karl-Heinz Glassmeier, Klaus Reinsch, Philipp Schulz, Sami Solanki

https://doi.org/10.5194/egusphere-2025-5536
Preprint. Discussion started: 3 December 2025

Competing interests. Conflict of Interest: The authors declare that the research was conducted in the absence of any commercial or financial relationships that could be construed as a potential conflict of interest.

Acknowledgements. The work of R. H. is funded by the "Hundred Talents Program" of the Chinese Academy of Sciences (CAS), and the "Excellent Young Scientists Fund Program (Overseas)" of the National Natural Science Foundation of China (NSFC).

https://doi.org/10.5194/egusphere-2025-5536
Preprint. Discussion started: 3 December 2025

References

Abraham-Shrauner, B.: Determination of magnetohydrodynamic shock normals. J. Geophys. Res. 77, 736–739, 1972. https://doi.org/10.1029/JA077i004p00736

Barbier, D.: L'activite aurorale aux basses latitudes. Annales de Geophysique, 14, 334–355, 1958.

Block, L. P.: A double layer review. Astrophys. Space Sci., 55, 59–83, 1978. https://doi.org/10.1007/BF00642580

Boardsen, S. A., Gallagher, D. L., Gurnett, D. A., Peterson, W. K., and Green, J. L.: Funnel-shaped, low-frequency equatorial waves. J. Geophys. Res. Space Physics, 97, 14,967–14,976, 1992. https://doi.org/10.1029/92JA00827

Carlson, C. W., and Kelley, M. C.: Observation and interpretation of particle and electric field measurements inside and adjacent to an active auroral arc. J. Geophys. Res. 82, 2349–2360, 1977. https://doi.org/10.1029/JA082i016p02349

Cole, K. D.: Stable auroral red arcs, sinks for energy of $D_{\rm st}$ main phase. J. Geophys. Res., 70, 1689–1706, 1965. https://doi.org/10.1029/JZ070i007p01689

Cornwall, J. M., Coroniti, F. V., and Thorne, R. M.: Turbulent loss of ring current protons. J. Geophys. Res., 75, 4699–4709, 1970. https://doi.org/10.1029/JA075i025p04699

Cornwall, J. M., Coroniti, F. V., and Thorne, R. M.: Unified theory of SAR arc formation at the plasmapause. J. Geophys. Res., 76, 4428–4445, 1971. https://doi.org/10.1029/JA076i019p04428

Dessler, A. J., and Parker, E. N.: Hydromagnetic theory of geomagnetic storms. J. Geophys. Res., 64, 2239–2252, 1959. https://doi.org/10.1029/JZ064i012p02239

Dungey, J. W.: Interplanetary magnetic field and the auroral zones. Phys. Rev. Lett., 6, 47–48, 1961. https://doi.org/10.1103/PhysRevLett.6.47

Echer, E., Gonzalez, W. D., and Tsurutani, B. T. Interplanetary conditions leading to superintense geomagnetic storms ($D_{\rm st} \leq -250$ nT) during solar cycle 23. Geophys. Res. Lett., 35, 2007GL031755. 2008. https://doi.org/10.1029/2007GL031755

Evans, D. S.: Precipitating electron fluxes formed by a magnetic field aligned potential difference. J. Geophys. Res., 79, 2853–2858, 1974. https://doi.org/10.1029/JA079i019p02853

Gjerloev, J. W.: A global ground-based magnetometer initiative. Eos, Transactions, American Geophysical Union, 90, 230–231, 2009. https://doi.org/10.1029/2009EO270002

Gjerloev, J. W. The SuperMAG data processing technique. J. Geophys. Res. Space Physics, 117, 2012JA017683, 2012. https://doi.org/10.1029/2012JA017683

Gurnett, D. A., Plasma wave interactions with energetic ions near the magnetic equator. J. Geophys. Res., 81, 2765–2770, 1976. https://doi.org/10.1029/JA081i016p02765

Hajra, R., Tsurutani, B. T., Lakhina, G. S., Lu, Q., and Du, A.: Interplanetary causes and impacts of the 2024 May superstorm on the geosphere: An Overview. Astrophys. J., 974, 264. 2024. https://doi.org/10.3847/1538-4357/ad7462

Hajra, R., Tsurutani, B. T., Lu, Q., Du, A., and Lakhina, G. S.: Supersubstorms during the May 2024 superstorm. J. Space Weather Space Clim., in press. https://doi.org/10.1051/swsc/2025047

Hasegawa, A.: Particle acceleration by MHD surface wave and formation of aurora. J. Geophys. Res, 81, 5083–5090. 1976. https://doi.org/10.1029/JA081i028p05083

Horne, R. B., Wheeler, G. V., and Alleyne, H. St. C. K.: Proton and electron heating by radially propagating fast magnetosonic waves. J. Geophys. Res. Space Physics, 105, 27,597–27,610. 2000. https://doi.org/10.1029/2000JA000018

https://doi.org/10.5194/egusphere-2025-5536
Preprint. Discussion started: 3 December 2025

Hugoniot, H.: Mémoire sur la propagation des mouvements dans les corps et spécialement dans les gaz parfaits (premiŕe partie). Journal de l'École Polytechnique, 57, 3–97, 1887.

Hugoniot, H.] Mémoire sur la propagation des mouvements dans les corps et spécialement dans les gaz parfaits (deuxiḿe partie), Journal de l'Éole Polytechnique, 58, 1–125, 1889.

Iyemori, T.: Storm-time magnetospheric currents inferred from mid-latitude geomagnetic field variations. J. Geomag. Geoelec., 42, 1249–1265, 1990. https://doi.org/10.5636/jgg.42.1249

King, J. H., and Papitashvili, N. E.: OMNI 1-min Data Set [Data set]. NASA Space Physics Data Facility, 2020. https://doi.org/10.48322/45BB-8792

Kozyra, J. U., Chandler, M. O., Hamilton, D. C., Peterson, W. K., Klumpar, D. M., Slater, D. W., et al.: The role of ring current nose events in producing stable auroral red arc intensifications during the main phase: Observations during the September 19–24, 1984, Equinox Transition Study. J. Geophys. Res. Space Physics, 98, 9267–9283. 1993. https://doi.org/10.1029/92JA02554

Lemaire, J., and Scherer, M.: Ionosphere-plasmasheet field-aligned currents and parallel electric fields. Planet. Space Sci., 22, 1485–1490, 1974. https://doi.org/10.1016/0032-0633(74)90013-0

Lummerzheim, D.: Modeling and forecasting aurora. Comp. Sci. Engineer., 9, 53–61, 2007. https://doi.org/10.1109/MCSE.2007.103

McIlwain, C. E.: Coordinates for mapping the distribution of magnetically trapped particles. J. Geophys. Res., 66, 3681–3691, 1961. https://doi.org/10.1029/JZ066i011p03681

Meredith, N. P., Horne, R. B., and Anderson, R. R.: Survey of magnetosonic waves and proton ring distributions in the Earth's inner magnetosphere. J. Geophys. Res. Space Physics, 113, 2007JA012975, 2008. https://doi.org/10.1029/2007JA012975

Němec, F., Santolík, O., Pickett, J. S., Hrbáčková, Z., and Cornilleau-Wehrlin, N.: Azimuthal directions of equatorial noise propagation determined using 10 years of data from the Cluster spacecraft. J. Geophys. Res. Space Physics, 118, 7160–7169, 2013. https://doi.org/10.1002/2013JA019373

Newell, P. T., and Gjerloev, J. W.: Evaluation of SuperMAG auroral electrojet indices as indicators of substorms and auroral power. J. Geophys. Res. Space Physics, 116, 2011JA016779. 2011. https://doi.org/10.1029/2011JA016779

Perraut, S., Roux, A., Robert, P., Gendrin, R., Sauvaud, J. A., Bosqued, J. M., et al.:. A systematic study of ULF waves above F_{H+} from GEOS 1 and 2 measurements and their relationships with proton ring distributions, J. Geophys. Res. Space Physics, 87, 6219–6236, 1982.. https://doi.org/10.1029/JA087iA08p06219

Pokhotelov, O. A., Sagdeev, R. Z., Balikhin, M. A., Onishchenko, O. G., and Fedun, V. N.: Nonlinear mirror waves in non-Maxwellian space plasmas. J. Geophys. Res. Space Physics, 113, 2007JA012642, 2008. https://doi.org/10.1029/2007JA012642

Rankine, W. J. M.: On the thermodynamic theory of waves of finite longitudinal disturbance. Phil. Trans. Royal Soc. London, 160, 277–288, 1870. https://doi.org/10.1098/rstl.1870.0015

Rees, M. H.: Physics and Chemistry of the Upper Atmosphere (1st ed.). Cambridge University Press, 1989. https://doi.org/10.1017/CBO9780511573118

Rees, M. H., Walker, J. C. G., and Dalgarno, A.: Auroral excitation of the forbidden lines of atomic oxygen. Planet. Space Sci., 15, 1097–1110, 1967. https://doi.org/10.1016/0032-0633(67)90096-7

Roach, F. E., and Marovich, E.: A monochromatic low-latitude aurora. J. Res. Nat. Bureau Standard, Section D: Radio Propagation, 63D, 297, 1959. https://doi.org/10.6028/jres.063D.029

Roach, F. E., and Roach, J. R.: Stable 6300 Åauroral arcs in mid-latitudes. Planet. Space Sci., 11, 523–549, 1963. https://doi.org/10.1016/0032-0633(63)90076-X

https://doi.org/10.5194/egusphere-2025-5536
Preprint. Discussion started: 3 December 2025

Santolík, O., Pickett, J. S., Gurnett, D. A., Maksimovic, M., and Cornilleau-Wehrlin, N.: Spatiotemporal variability and propagation of equatorial noise observed by Cluster. J. Geophys. Res. Space Physics, 107, 1495, 2002. https://doi.org/10.1029/2001JA009159

Schriver, D., Ashour-Abdalla, M., Strangeway, R. J., Richard, R. L., Klezting, C., Dotan, Y., and Wygant, J.: FAST/Polar conjunction study of field-aligned auroral acceleration and corresponding magnetotail drivers. J. Geophys. Res. Space Physics, 108, 2002JA009426. 2003. https://doi.org/10.1029/2002JA009426

Sckopke, N.: A general relation between the energy of trapped particles and the disturbance field near the Earth. J. Geophys. Res., 71, 3125–3130, 1966. https://doi.org/10.1029/JZ071i013p03125

Smith, E. J., Frandsen, A. M. A., Tsurutani, B. T., Thorne, R. M., and Chan, K. W.. Plasmaspheric hiss intensity variations during magnetic storms. J. Geophys. Res., 79, 2507–2510, 1974. https://doi.org/10.1029/JA079i016p02507

Thorne, R. M.: Radiation belt dynamics: The importance of wave-particle interactions, Geophys. Res. Lett., 37, 2010GL044990, 2010. https://doi.org/10.1029/2010GL044990

Tsurutani, B. T., and Gonzalez, W. D.: A new perspective on the relationship between substorms and magnetic storms, in Geosciences (Vol. 8: Solar Terrestrial (ST), pp. 25–45). 5 Toh Tuck Link, Singapore 596224: World Scientific Publishing, 2007. https://doi.org/10.1142/9789812708939_0002

Tsurutani, B. T., and Lakhina, G. S.: An extreme coronal mass ejection and consequences for the magnetosphere and Earth, Geophys. Res. Lett. 41, 287–292. 2014. https://doi.org/10.1002/2013GL058825

Tsurutani, B. T., Gonzalez, W. D., Tang, F., Akasofu, S.-I., and Smith, E. J.: Origin of interplanetary southward magnetic fields responsible for major magnetic storms near solar maximum (1978–1979), J. Geophys. Res. Space Physics, 93, 8519–8531, 1988. https://doi.org/10.1029/JA093iA08p08519

Tsurutani, B. T., Gonzalez, W. D., Lakhina, G. S., and Alex, S.: The extreme magnetic storm of 1–2 September 1859. J. Geophys. Res. Space Physics, 108, 2002JA009504. 2003. https://doi.org/10.1029/2002JA009504

Tsurutani, B. T., Falkowski, B. J., Pickett, J. S., Verkhoglyadova, O. P., Santolik, O., and Lakhina, G. S.: Extremely intense ELF magnetosonic waves: A survey of polar observations. J. Geophys. Res. Space Physics, 119, 964–977. 2014. https://doi.org/10.1002/2013JA019284

Tsurutani, B. T., Hajra, R., Echer, E., and Gjerloev, J. W.: Extremely intense ($\mathrm{SML} \leq -2500\ \mathrm{nT}$) substorms: isolated events that are externally triggered? Ann. Geophys., 33, 519–524, 2015. https://doi.org/10.5194/angeo-33-519-2015